Journal of Porphyrins and Phthalocyanines
J. Porphyrins Phthalocyanines 2017; **21**: 1–8
DOI: 10.1142/S1088424617500936

Published at http://www.worldscinet.com/jpp/

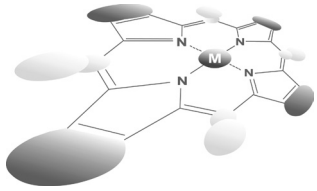

Substitution of an amino acid residue axially coordinating to the heme molecule in hexameric tyrosine-coordinated hemoprotein to enhance peroxidase activity

Tsuyoshi Mashima[a], Koji Oohora*[a,b,c◊] and Takashi Hayashi*[a◊]

[a] *Department of Applied Chemistry, Graduate School of Engineering, Osaka University, Suita 565-0871, Japan*
[b] *Frontier Research Base for Global Young Researchers, Graduate School of Engineering, Osaka University, 2-1 Yamadaoka, Suita, 565-0871, Japan*
[c] *PRESTO, Japan Science and Technology Agency, 4-1-8 Honcho, Kawaguchi 332-0012, Japan*

Received 22 November 2017
Accepted 3 December 2017

ABSTRACT: To convert an originally tyrosine-coordinated heme to histidine-coordinated heme in hexameric tyrosine-coordinated hemoprotein, HTHP, Tyr45, a residue coordinating to the heme cofactor, and Arg25 located in the distal site are replaced with Phe45 and His25, respectively in each of the subunits of the protein. The obtained HTHP mutant ($HTHP^{R25H/Y45F}$) was characterized by SDS-PAGE, ESI-TOF MS, dynamic light scattering measurements and size exclusion chromatography. These analyses indicate that $HTHP^{R25H/Y45F}$ maintains its stable hexameric structure with the altered ligation of each of the heme cofactors. Comparison of UV-vis absorption spectra of the ferric-, ferrous-, CO- and CN-forms of $HTHP^{R25H/Y45F}$ with those of several well-known His-ligated hemoproteins indicates that heme is coordinated by the His25 residue. The reaction of $HTHP^{R25H/Y45F}$ with cumene hydroperoxide produces both cumyl alcohol and acetophenone in a 2.3:1 ratio, indicating that heterolytic O–O bond cleavage dominantly occurs to form the two-electron oxidized species known as compound I. Peroxidase activity of $HTHP^{R25H/Y45F}$ is found to follow Michaelis–Menten kinetics. The k_{cat} values of $HTHP^{R25H/Y45F}$ for H_2O_2-dependent oxidation of ABTS and guaiacol are 10- and 100-fold higher, respectively, than those of wild type HTHP ($HTHP^{WT}$). The k_{cat}/K_m values of $HTHP^{R25H/Y45F}$ for both substrates are increased 30-fold relative to that of $HTHP^{WT}$. Moreover, $HTHP^{R25H/Y45F}$ is capable of promoting catalytic sulfoxidation of thioanisole with H_2O_2 with a turnover number *ca*. 2-fold higher than that of $HTHP^{WT}$. The present findings demonstrate that proximal His ligation to the heme is significantly effective to increase the peroxidase activity in the HTHP matrix.

KEYWORDS: hemoprotein, peroxidase, hexamer.

INTRODUCTION

Hemoproteins are responsible for several important functions in biological systems such as oxygen storage and transport, gas sensing, electron transfer, and metabolism *via* oxidation and oxygenation [1–3]. Despite using the same cofactor, the protein matrices impose a range of physicochemical properties to induce specific reactivities which support these sophisticated functions. In other words, the reactivity of a given heme cofactor within a hemoenzyme is essentially controlled by the protein matrix. Axially coordinated amino acid residues in the heme pocket are a prime example of such protein matrix control [4, 5]. Wide ranging investigations of hemoprotein chemistry over the past half century have indicated that the functional groups of histidine, cysteine, and tyrosine are the primary axial heme ligands [6]. Histidine is a common residue coordinating to heme in peroxidases as well as oxygen-binding hemoproteins

◊ SPP full member in good standing

*Correspondence to: Koji Oohora, email: oohora@chem.eng.osaka-u.ac.jp; Takashi Hayashi, email: thayashi@chem.eng.osaka-u.ac.jp.

such as myoglobin (Mb) and hemoglobin [7–9]. In the case of horseradish peroxidase, the coordinated imidazole functional group of the histidine residue forms a hydrogen bond with an aspartic acid group to afford imidazolate-like coordination, which induces efficient formation of the high valent reactive intermediate, compound I species (Fe^{IV}-oxo porphyrin π-cation radical) in a reaction with hydrogen peroxide [10, 11]. Cytochrome P450s, which are heme-dependent monooxygenases, employ cysteine as the axial ligand [12, 13]. The strong push-effect and the radical character in the compound I species collectively enable highly efficient activation of inert C–H bonds. Tyrosine is axially coordinated to heme in catalase, which promotes the disproportionation of hydrogen peroxide [14, 15]. The phenolate-type coordination to the heme provided by the tyrosine side chain also appears to provide a strong push-effect for the formation of a compound I species. Thus, the axial ligand is extremely important for regulating the reactivity of high-valent catalytic species, and mutations focusing on axial ligands in hemoproteins have been investigated [16–23].

Hexameric tyrosine-coordinated heme protein, HTHP, from the marine bacterium *Silicibacter pomeroyi* is a thermally stable homo-hexameric hemoprotein composed only of α helices (Fig. 1a) [24]. HTHP has a heme molecule in each subunit which is coordinated by Tyr45 as an axial ligand to form a five-coordinate structure (Fig. 1b). In the distal site of the heme pocket, Arg25 interacts with heme *via* a π-cation interaction. The peroxidase and catalase activities of HTHP are relatively low compared with typical peroxidase and catalase activities. In contrast to these enzymes, the heme in HTHP is highly exposed to solvent [24]. Although the native function of HTHP remains unknown, its rigid and highly-symmetric structure is attractive for engineering of protein functions [25]. In the present work, we focus on proximal ligation of heme for modification of HTHP and demonstrate that substitution of the axial ligand from tyrosine to histidine enhances the peroxidase activity of HTHP (Fig. 1b).

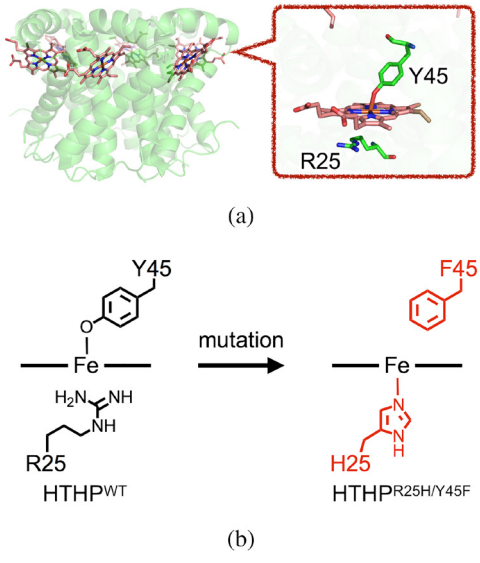

Fig. 1. (a) Crystal structure of HTHP^{WT} (PDB ID: 2OYY). (b) Schematic heme pocket structure of HTHP^{WT} and HTHP$^{R25H/Y45F}$

EXPERIMENTAL METHODS

Instruments

UV-vis spectral measurements were carried out with a UV-2700 double-beam spectrophotometer (Shimadzu), a V-670 UV-vis-NIR spectrophotometer (JASCO) or a BioSpec-nano spectrophotometer (Shimadzu). ESI-TOF MS analysis was performed with a Bruker Daltonics micrOTOF-II mass spectrometer. The pH measurements were made with an F-52 Horiba pH meter. Size exclusion chromatography was performed using an ÄKTA purifier system equipped with a Superdex 200 Increase 10/300 GL column (GE Healthcare) at 4 °C. Dynamic light scattering was measured using a Malvern Zetasizer μV light scattering analyzer with an 830 nm laser at 25 °C. HPLC analysis was conducted with a Shimadzu HPLC Prominence system equipped with a YMC-Triart C18 column (150 × 4.6 mm I.D.). The measurements for evaluation of peroxidase activity were conducted with a rapid scan stopped-flow system (Unisoku) using a Xe or halogen light source. The GC/FID measurements were made with a Shimadzu GC-2010 gas chromatography system.

Materials

Ultrapure water (Milli-Q) was prepared using a Millipore Integral 3 apparatus. Other all chemicals were of the highest guaranteed grade commercially available and were used as received unless otherwise indicated. Mb and horseradish peroxidase (HRP), were purchased from Sigma Aldrich and Wako, respectively.

Amino acid sequence of the monomers of HTHP^{WT} and HTHP$^{R25H/Y45F}$

HTHP^{WT};

SETWLPTLVTATPQEGFDLAVKLSRIAVKKTQPD-AQVRDTLRAVYEKDANALIAVSAVVATHFQTIAA-ANDYWKD

HTHP$^{R25H/Y45F}$;

SETWLPTLVTATPQEGFDLAVKLSHIAVKKTQPDA-QVRDTLRAVFEKDANALIAVSAVVATHFQTIAAA-NDYWKD

Expression and purification of HTHP$^{R25H/Y45F}$

The gene expression system for HTHP^{WT} was reported in our previous paper [25]. Site-directed mutagenesis was

performed using the polymerase chain reaction (PCR) and the LA PCR *in vitro* Mutagenesis Kit (Takara) according to the manufacturer's protocol. The HTHP gene cloned into pDEST14 was used as a template to introduce mutations into the HTHP matrix with primers (i). After PCR, the template DNA plasmids were digested with Dpn I (Thermo Fisher Scientific). *E. coli* DH5α competent cells were transformed with the PCR products. After cultivation, the plasmids were purified with PureLink™ Quick Plasmid Miniprep Kit (Thermo Fisher Scientific). The obtained plasmid was further used as a template for site-directed mutagenesis with the primers (ii). The desired plasmid containing the gene for the double mutant of HTHP (R25H/Y45F) was obtained using the same method.

DNA sequencing was performed to verify each correct mutation in the gene sequence.

The primer sequences used to generate the mutant were:

(i) R25H: (5′-GGCCGTGAAACTGTCGCACATTGC-GGTCAAGAAAAC-3′) and the complementary primer;
(ii) Y45F: (5′-GCGATACTCTCCGTGCTGTGTTCGA-GAAAGATGCGAATGCGCTG-3′) and the complementary primer.

The resulting expression plasmid was used to transform *E. coli* BL21 (DE3). LB medium (4 L) containing ampicillin (400 mg) was inoculated with 50 mL of the culture (OD = 0.5) of the transformed cells. After the cells were grown aerobically with vigorous shaking at 37 °C until OD600 was reached ~0.5, isopropyl-β-D-1-thiogalactopyranoside (IPTG, final concentration: 1 mM) was added to the culture for induction of protein expression. The culture was continued at 37 °C overnight. The cells were harvested by centrifugation at 4000 × g for 10 min. The harvested cells from 4 L of culture were re-suspended in *ca*. 50 mL of a 10 mM Tris-HCl buffer, pH 8.0, and lysed by freeze-thaw cycles with subsequent sonication for 30 s × 10 times at 4 °C. The lysate was then centrifuged and the supernatant was collected. The solution was diluted 10-fold with 100 mM potassium phosphate buffer at pH 7.0 and loaded through a CM Fast Flow (GE Healthcare) cation-exchange column pre-equilibrated with 100 mM potassium phosphate buffer at pH 7.0. The flow-through solution was loaded onto a DEAE Fast Flow (GE Healthcare) anion-exchange column pre-equilibrated with 100 mM potassium phosphate buffer at pH 7.0. The fraction of the target protein was collected with a 100 mM potassium phosphate buffer at pH 7.0 containing 0.3 M NaCl. The obtained solution was concentrated using an Amicon stirred ultrafiltration cell with a 30-kDa molecular weight cut-off membrane (Millipore). The concentrated solution was passed through a Superdex 200 Increase 10/300 GL column with 100 mM potassium phosphate buffer at pH 6.0. The fractions with $R_z > 2$ (R_z is a ratio of absorbance values at 402 nm and 280 nm) were collected and loaded on a Hitrap Q HP 5 mL (GE Healthcare) anion-exchange column pre-equilibrated with 100 mM potassium phosphate buffer at pH 6.0. The fraction of the target protein was eluted with 100 mM potassium phosphate buffer at pH 6.0 containing 0.35 M NaCl. The obtained HTHP mutant ($HTHP^{R25H/Y45F}$) was characterized by SDS-PAGE (Fig. 2), ESI-TOF MS (Fig. 3), analytical size exclusion chromatography (SEC, Fig. 4), and UV-vis spectroscopy (Fig. 5a), and stored at -80 °C. The concentration of heme was determined by characteristic absorbance as a pyridine hemochrome complex (ε_{556} = 34.4 $mM^{-1} \cdot cm^{-1}$). The extinction coefficient (ε_{405} = 111 $mM^{-1} \cdot cm^{-1}$) of $HTHP^{R25H/Y45F}$ was determined from the plots of the absorbance at 405 nm of $HTHP^{R25H/Y45F}$ for the concentration of heme (Fig. S1).

Analytical size exclusion chromatography

For SEC analysis, 100 mM potassium phosphate buffer at pH 7.0 was used as an eluent. The analysis was performed at 4 °C and a flow rate of 0.5 $mL \cdot min^{-1}$ with monitoring of the absorbance at 280 and 400 nm for detection. The Superdex 200 column was calibrated using the following reagents: ferritin (400 kDa), albumin (67 kDa), ovalbumin (40 kDa), and chymotrypsinogen (25 kDa).

Preparation of ferrous-, CO- and cyanide-forms of $HTHP^{WT}$ and $HTHP^{R25H/Y45F}$

To obtain the ferrous-forms of $HTHP^{WT}$ and $HTHP^{R25H/Y45F}$, a small excess amount of $Na_2S_2O_4$ was added to the protein solution. The CO-forms were prepared by bubbling the ferrous-form solutions with CO gas for 2 min. To solutions of ferrous-$HTHP^{WT}$ and ferric $HTHP^{R25H/Y45F}$ in 100 mM potassium phosphate buffer at pH 7.0 potassium cyanide solution was added (final concentration: 10 mM), giving cyanide-ferrous $HTHP^{WT}$ and cyanide-ferric $HTHP^{R25H/Y45F}$, respectively.

Reaction of $HTHP^{WT}$ and $HTHP^{R25H/Y45F}$ with cumene hydroperoxide

A cumene hydroperoxide, CHPO, solution was added to the protein solution ([protein] = 20 μM, [CHPO] = 2 mM, 100 μL) in 100 mM potassium phosphate buffer at pH 7.0 and 25 °C for 2 h. The reaction mixture was filtered using a Millix®-GV filter (0.22 μm), and the filtrate was analyzed using an HPLC system equipped with a C18 column to determine the amounts of produced acetophenone and cumyl alcohol.

Peroxidase activity

A mixture of protein (2 μM) and substrate dissolved in 100 mM potassium phosphate buffer at pH 7.0 was incubated at 25 °C for 10 min. UV-vis spectral changes

were recorded upon addition of H_2O_{2aq} (10 mM). The final concentrations of guaiacol or ABTS as a substrate were from 0.05 to 1.5 mM. After mixing the same volume (125 μL) of these two solutions, absorbance changes were recorded and the initial rates within 1 s were determined using the extinction coefficients of the oxidized products: ε_{470} = 26.6 $mM^{-1} \cdot cm^{-1}$ for guaiacol and ε_{728} = 15.0 $mM^{-1} \cdot cm^{-1}$ for ABTS. The plots of initial rates, v, per protein against substrate concentration were fitted with the following Michaelis–Menten equation to estimate the kinetic parameters for the oxidation reactions.

$$\frac{v}{[\text{protein}]} = \frac{k_{\text{cat}}[\text{substrate}]}{K_{\text{m}} + [\text{substrate}]}$$

Sulfoxidation of thioanisole

The reactions were carried out in 100 mM potassium phosphate buffer at pH 7.0 and 25 °C. A buffer solution of protein and thioanisole was incubated prior to the addition of H_2O_2 to initiate the reaction. The final concentrations of each component was follows: [protein] = 10 μM, [thioanisole] = 2.0 mM and [H_2O_2] = 1 mM. After the reaction was complete at 12 h, benzyl alcohol as an internal standard and ether were added, and the reaction mixture was vigorously shaken using a vortex mixer to extract the organic materials. The separated organic phase was evaporated by N_2 gas flow, dissolved in CH_3CN and analyzed with a GC/FID system equipped with a DB-1 column.

RESULTS AND DISCUSSION

Mutant design

The crystal structure of $HTHP^{WT}$ suggests that direct replacement of Tyr45, an axial ligand to the heme molecule in the protein, with His45 is inappropriate for constructing a His-coordinating hemoprotein, because the distance between the heme Fe ion and the α-carbon of the axially coordinated residue Tyr in the protein is significantly longer than the analogous distance observed in a series of His-coordinated hemoproteins. In contrast, it is found that Arg25 in the distal site of the heme pocket is relatively close to the heme iron: the distances from Cα (Tyr45) or Cα (Arg25) to Fe (heme) in $HTTP^{WT}$ are 8.5 and 5.8 Å, respectively (PDB ID: 2OYY [24]), whereas the distances from Cα (His93) or Cα (His64) to Fe (heme) in Mb are 6.6 and 8.6 Å, respectively (PDB ID: 1YMB [26]). Therefore, we prepared a double mutant $HTHP^{R25H/Y45F}$ where Tyr45 and Arg25 were replaced with Phe45 and His25, respectively. As a result, the engineering allows swapping of proximal and distal sites in this hemoprotein as shown in Fig. 1b.

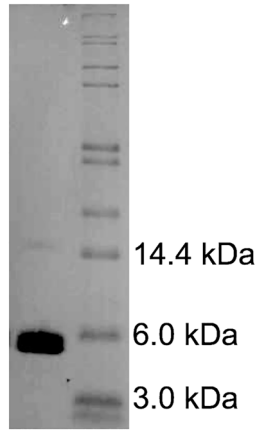

Fig. 2. SDS-PAGE electrophoretogram of $HTHP^{R25H/Y45F}$ (left lane) and several protein standard markers (right lane)

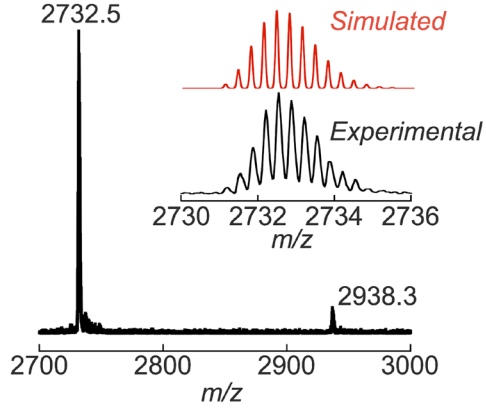

Fig. 3. ESI-TOF mass spectrum of the monomer of $HTHP^{R25H/Y45F}$. The sample was dissolved in 10 mM NH_4OAc aqueous solution at pH 6.9. Multiply ionized species were observed: found m/z = 2732.5 and 2938.3; calcd m/z = 2732.4 (z = 3+, apo-form) and 2938.2 (z = 3+, holo-form). Inset: The simulated (red, upper) and experimental (black, lower) isotopic distribution patterns for $[C_{370}H_{582}N_{98}O_{112}]^{3+}$ + $3H^+$ (z = 3+, monomer of apo-form of $HTHP^{R25H/Y45F}$)

Purification and characterization of $HTHP^{R25H/Y45F}$

$HTHP^{R25H/Y45F}$ was expressed in a recombinant *E. coli* system and purified by ion exchange chromatography and SEC. The purity of $HTHP^{R25H/Y45F}$ isolated from cultured cells was confirmed by SDS-PAGE (Fig. 2). The band of $HTHP^{R25H/Y45F}$ was only at about 6 kDa, which is consistent with the molecular weight of the monomer of $HTHP^{R25H/Y45F}$. This is an expected result because $HTHP^{R25H/Y45F}$ disassembles to the apo-form monomer in the presence of SDS. ESI-TOF MS (Fig. 3) shows the desired mass numbers of the multiply-ionized apo- and holo-forms of the monomer: found m/z = 2732.5 and 2938.3; calcd m/z = 2732.4 (z = 3+, apo-form) and 2938.2 (z = 3+, holo-form). The observed isotopic pattern of the apo-form (z = 3+) matched well with the simulated pattern. Dynamic light scattering measurements revealed

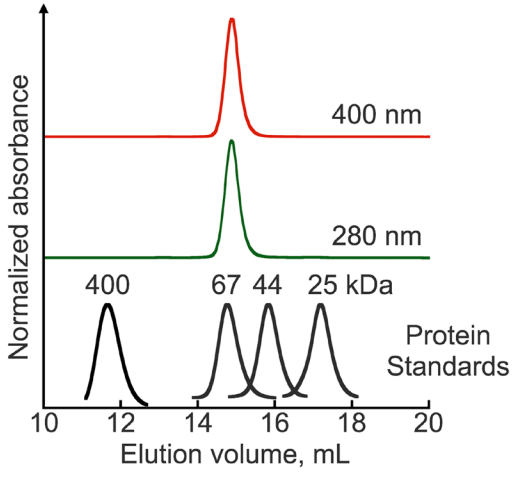

Fig. 4. Analytical SEC traces of HTHP$^{R25H/Y45F}$ and various protein standards. Traces of HTHP$^{R25H/Y45F}$ were observed at 400 and 280 nm, and traces of the protein standards were monitored at 280 nm

a monodispersed species with a hydrodynamic diameter of 6.26 nm, which is consistent with the value expected from the reported crystal structure of HTHP^{WT} [24]. Support for the formation of the hexameric structure in solution is also provided by analytical SEC with several protein standards as shown in Fig. 4: the elution volume of HTHP$^{R25H/Y45F}$ at 14.9 mL indicates a molecular weight of approximately 50 kDa. Furthermore, the SEC trace for HTHP$^{R25H/Y45F}$ monitored by measuring absorbance at 280 nm (for protein matrices) is clearly consistent with that monitored at 400 nm (for heme), indicating that the heme molecules are bound to the matrix of HTHP$^{R25H/Y45F}$.

UV-vis spectroscopic study

The UV-vis absorption spectra of several states of HTHP$^{R25H/Y45F}$ and HTHP^{WT} are shown in Fig. 5. The spectrum of as-isolated HTHP$^{R25H/Y45F}$ is almost identical to that of HTHP^{WT}, although the peak of the Q-band at 528 nm in HTHP^{WT} is absent in the spectrum of HTHP$^{R25H/Y45F}$. Interestingly, a similar result has also been observed in the engineered heme-binding human serum albumin (HSA$^{I142H/Y161L}$) where the proximal and distal sites are swapped in a double mutation (Table 1) [19, 27]. These findings support the evidence indicating that the heme pocket of HTHP$^{R25H/Y45F}$ provides a coordination environment which is similar to that of His-ligated heme-binding HSA$^{I142H/Y161L}$. Additionally, the characteristic features of the spectrum of HTHP$^{R25H/Y45F}$ are almost identical to those of wild type met-Mb with high-spin ferric heme, which has a His residue as an axial ligand. Reduction of HTHP$^{R25H/Y45F}$ upon addition of a small

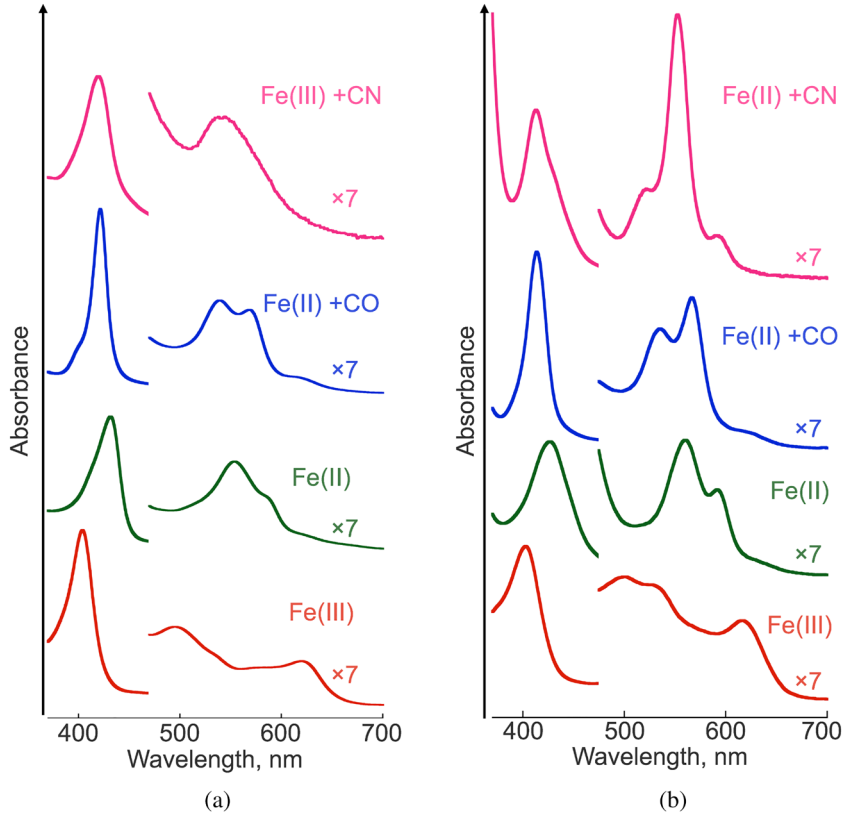

Fig. 5. UV-vis absorption spectra of ferric, ferrous, CO- and CN-forms of (a) HTHP$^{R25H/Y45F}$ and (b) HTHP^{WT} in 100 mM potassium phosphate buffer at pH 7.0 and 25 °C

Table 1. λ_{max} in the UV-vis absorption spectra of $HTHP^{WT}$, $HTHP^{R25H/Y45F}$ and reported hemoproteins

Protein	State	λ_{max} at Soret band (nm)	λ_{max} at Q-band (nm)
$HTHP^{WT}$	Fe^{3+}	402	501, 528, 616
	Fe^{2+}	431	560, 592
	Fe^{2+} + CO	420	535, 566
	Fe^{2+} + CN	413	523, 553, 591
$HTHP^{R25H/Y45F}$	Fe^{3+}	405	495, 620
	Fe^{2+}	432	554, 589(sh),
	Fe^{2+} + CO	421	539, 568, 615 (sh)
	Fe^{3+} + CN	420	542
heme-binding HSA^{WT}[a]	Fe^{3+}	405	501, 534, 624
	Fe^{2+}	419	538, 559 (sh), 570
	Fe^{2+} + CO	416	539, 568
heme-binding $HSA^{I142H/Y161L}$[a]	Fe^{3+}	402	533, 620
	Fe^{2+}	426	531 (sh), 559
	Fe^{2+} + CO	419	538, 565
Mb[a]	Fe^{3+}	409	503, 548 (sh), 632
	Fe^{2+}	434	557
	Fe^{2+} + CO	423	541, 579

[a] Reference [27].

Table 2. Kinetics parameters of $HTHP^{WT}$ and $HTHP^{R25H/Y45F}$ from the Michaelis-Menten equation for the oxidation of ABTS[a]

Protein	k_{cat} (s^{-1})	K_m (mM)	k_{cat}/K_m ($mM^{-1} \cdot s^{-1}$)
$HTHP^{WT}$	0.54	0.12	4.5
$HTHP^{R25H/Y45F}$	5.2	3.8×10^{-2}	1.4×10^{2}
HRP[b]	4.0×10^{2}	5.8	5.1×10^{3}

[a] Reaction conditions: [protein] = 1 μM, [H_2O_2] = 5 mM, [ABTS] = 0.05 to 1 mM in 100 mM potassium phosphate buffer at pH 7.0 and 25 °C. [b] Figure S2a.

Table 3. Kinetics parameters of $HTHP^{WT}$ and $HTHP^{R25H/Y45F}$ from the Michaelis-Menten equation for the oxidation of guaiacol[a]

Protein	k_{cat} (s^{-1})	K_m (mM)	k_{cat}/K_m ($mM^{-1} \cdot s^{-1}$)
$HTHP^{WT}$	3.0×10^{-2}	0.11	0.27
$HTHP^{R25H/Y45F}$	2.8	0.34	8.1
HRP[b]	5.5×10^{2}	6.0	92

[a] Reaction conditions: [protein] = 1 μM, [H_2O_2] = 5 mM, [Guaiacol] = 0.05 to 1.5 mM in 100 mM potassium phosphate buffer at pH 7.0 and 25 °C. [b] Figure S2b.

excess of $Na_2S_2O_4$ affords the characteristic red-shift of the Soret band (Fig. 5) which is seen for Mb and heme-binding $HSA^{I142H/Y161L}$, indicating the formation of deoxy $HTHP^{R25H/Y45F}$ which has a His-ligated five-coordinate structure [27]. Next, bubbling of CO into the sample of deoxy $HTHP^{R25H/Y45F}$ yields a sharp Soret band at 420 nm and two peaks in the Q-band region (Fig. 5a and Table 1). These are typical features of CO-ligated heme as seen in heme-binding $HSA^{I142H/Y161L}$ and Mb. The addition of potassium cyanide to ferric $HTHP^{R25H/Y45F}$ also produces clear spectral changes of the Soret and Q-band as shown in the formation of cyanide complex of met-Mb [28]. This behavior is sharply different from that observed for $HTHP^{WT}$: the wild type ferric protein with the Tyr ligand does not bind cyanide [24]. Taken together, these results indicate that the introduced His25 residue undoubtedly coordinates to the heme iron in the heme pocket of $HTHP^{R25H/Y45F}$, since $HTHP^{R25H/Y45F}$ does not have other accessible His residues in the protein matrix.

Reaction with cumene hydroperoxide

To evaluate the reaction behavior of ferric $HTHP^{R25H/Y45F}$ with hydroperoxide, the O–O bond cleavage of cumene hydroperoxide (CHPO) was investigated. In this reaction, it is known that two possible products, cumyl alcohol and acetophenone, are produced after protein-assisted heterolytic and homolytic cleavage of the O–O

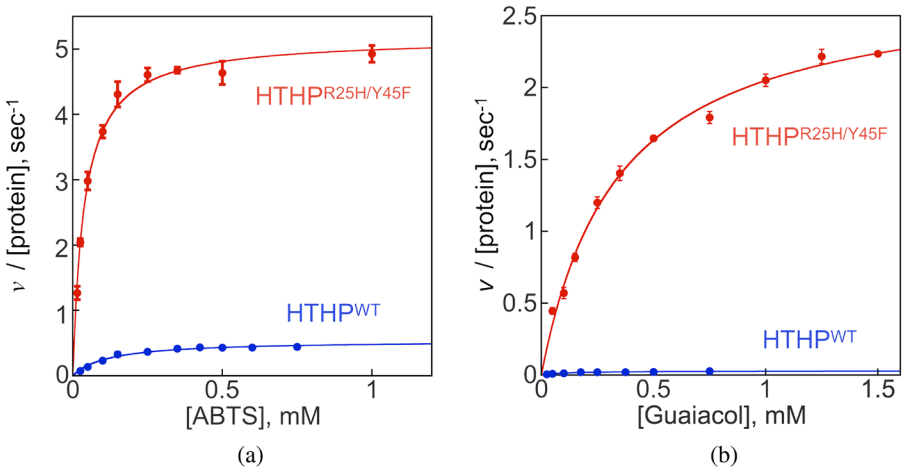

Fig. 6. Michaelis-Menten plots for (a) ABTS and (b) guaiacol oxidations catalyzed by $HTHP^{R25H/Y45F}$ and $HTHP^{WT}$. Conditions: [protein] = 1 μM, [H_2O_2] = 5 mM in 100 mM potassium phosphate buffer at pH 7.0 and 25 °C

bond, respectively. The product ratio (cumyl alcohol/acetophenone) provided by $HTHP^{R25H/Y45F}$ was determined to be 2.3 ± 0.3, whereas the ratio of Mb was reported to be 3.3 [29]. The obtained lower ratio for $HTHP^{R25H/Y45F}$ indicates that approximately 1/3 heme-peroxide provides the oxoferryl species (Fe(IV)=O), compound II, *via* O–O bond homolysis. These findings suggest that the push-effect of the proximal His to the heme in $HTHP^{R25H/Y45F}$ is lower than that of Mb. In contrast, it is found that $HTHP^{WT}$ does not react with CHPO.

Peroxidase activity of $HTHP^{R25H/Y45F}$

The steady-state kinetics of ABTS and guaiacol oxidation by $HTHP^{R25H/Y45F}$ and $HTHP^{WT}$ were evaluated to understand the effects of the axial ligand substitution on peroxidase activity. After addition of H_2O_2 to a solution of $HTHP^{R25H/Y45F}$ or $HTHP^{WT}$ containing the substrate, the absorbance changes derived from the resulting products were observed. The initial reaction rates (υ) were used to determine the values of Michaelis–Menten kinetic parameters, k_{cat} and K_m (Fig. 6 and Tables 2, 3).

The k_{cat} values of $HTHP^{R25H/Y45F}$ for ABTS and guaiacol oxidation are 10- and 100-fold higher than those of $HTHP^{WT}$, respectively. It is possible that the improvement of the peroxidase activity is due to the substitution of the axial ligand. However, the k_{cat} value of $HTHP^{R25H/Y45F}$ was found to be much lower than that of HRP, primarily because $HTHP^{R25H/Y45F}$ lacks the imidazolate-formed proximal His and distal His supporting the H_2O_2 activation. The K_m values for the ABTS and guaiacol oxidation reactions with $HTHP^{R25H/Y45F}$ are only 3-fold lower and higher than those of $HTHP^{WT}$, respectively. The present modification of HTHP does not significantly affect the affinity between the substrates and protein. The values of overall catalytic efficiency, k_{cat}/K_m, of $HTHP^{R25H/Y45F}$ are 30-fold higher than that of $HTHP^{WT}$ for both substrates, suggesting that the replacement of the tyrosine axial ligand with histidine clearly enhances peroxidase activity of $HTHP^{WT}$.

Sulfoxidation activity of $HTHP^{R25H/Y45F}$

To evaluate the two-electron oxidation ability of $HTHP^{R25H/Y45F}$ and $HTHP^{WT}$, thioanisole was employed as a substrate for an H_2O_2-dependent sulfoxidation reaction. The turnover numbers of $HTHP^{R25H/Y45F}$ and $HTHP^{WT}$ were found to be 43 and 23, respectively, at pH 7.0. Over-oxidation products such as sulfone were not detected after 12 h. These results indicate that axial-ligand substitution in HTHP is also effective for promotion of catalytic sulfoxidation.

CONCLUSION

$HTHP^{R25H/Y45F}$, a double mutant of HTHP designed to exchange the native Tyr axial ligand with His, was prepared and characterized. Analytical size exclusion chromatography and dynamic light scattering measurements revealed that $HTHP^{R25H/Y45F}$ maintains its intrinsic hexameric structure with bound heme molecules even though swapping of the proximal and distal sites in the protein matrix was carried out. His-ligation in $HTHP^{R25H/Y45F}$ is clearly supported by UV-vis spectra of as-isolated and reduced $HTHP^{R25H/Y45F}$. $HTHP^{R25H/Y45F}$ also has typical UV-vis spectra of CO- and CN-bound hemoproteins with His-ligation.

It is known that axial-ligand exchange by mutagenesis can cause significant perturbations of the physicochemical properties and reactivities of hemoproteins. In the present study, the His-ligating $HTHP^{R25H/Y45F}$ clearly shows higher catalytic efficiency toward ABTS, guaiacol oxidation and thioanisole sulfoxidation compared to that of the wild type protein. These results indicate that hemoprotein engineering focusing on axial ligand exchange will serve as a useful strategy for development of new biocatalysts.

Acknowledgments

This work was supported by Grants-in-Aid for Scientific Research provided by JSPS KAKENHI Grant Numbers JP15H05804, JP15H00873, JP16K14036, JP16H06045, and JP16H00837. We appreciate the support from JST PRESTO (JPMJPR15S2), JST SICORP and Osaka University International Joint Research Promotion Program. T.M. appreciates support from the JSPS Research Fellowship for Young Scientists (JSPS KAKENHI Grant Number JP15J00743).

REFERENCES

1. Phillips GN Jr, *Handbook of Metalloproteins*, Vol. 1, Messerschmidt A, Huber R, Poulos T and Wieghardt K, (Eds.); John Wiley & Sons: Chichester, U.K., 2001.
2. Paoli M, Marles-Wright J and Smith A. *DNA Cell Biol.* 2002; **4**: 271–280.
3. Chapman SK, Daff S and Munro AW. *Struct. Bond.* 1997; **88**: 39–70.
4. Dawson JH. *Science* 1988; **240**: 433–439.
5. Poulos TL. *J. Biol. Inorg. Chem.* 1996; **1**: 356–359.
6. Reedy CJ and Gibney BR. *Chem. Rev.* 2004; **104**: 617−649.
7. Springer BA, Sligar SG, Olson JS and Phillips GN Jr. *Chem. Rev.* 1994; **94**: 699–714.
8. Perutz MF. *Nature* 1970; **228**: 726–734.
9. Shaanan B. *J. Mol. Biol.* 1983; **171**: 31–59.
10. Dunford HB and Stillman JS. *Coord. Chem. Rev.* 1976; **19**: 187–251.
11. Berglund GI, Carlsson GH, Smith AT, Szöke H, Henriksen A and Hajdu J. *Nature* 2002; **417**: 463–468.
12. Ortiz de Montellano RP. *Chem. Rev.* 2010; **110**: 932–948.
13. Denisov IG, Makris TM, Sligar SG and Schlichting I. *Chem. Rev.* 2005; **105**: 2253−2277.
14. Zamocky M and Koller F. *Progr. Biophys. Mol. Biol.* 1999; **72**: 19–66.
15. Fita I and Rossmann MG. *J. Mol. Biol.* 1985; **185**: 21–37.
16. Sato H, Hayashi T, Ando T, Hisaeda Y, Ueno T and Watanabe Y. *J. Am. Chem. Soc.* 2004; **126**: 436–437.
17. Barrick D. *Biochemistry* 1994; **33**: 6546–6554.
18. Onderko EL, Silakov A, Yosca TH and Green MT. *Nat. Chem.* 2017; **9**: 623–628.
19. Komatsu T, Ohmichi N, Zunszain PA, Curry S and Tsuchida E. *J. Am. Chem. Soc.* 2004; **126**: 14304–14305.
20. Watanabe K, Ishikawa N and Komatsu T. *Chem. Asian J.* 2012; **7**: 2534–2537.
21. Sun J, Fitzgerald MM, Goodin DB and Loehr TM. *J. Am. Chem. Soc.* 1997; **119**: 2064–2065.
22. Adachi S, Nagano S, Ishimori K, Watanabe Y, Morishima I, Egawa T, Kitagawa T and Makino R. *Biochemistry* 1993; **32**: 241–252.
23. Du J, Sono M and Dawson JH. *Coord. Chem. Rev.* 2011; **255**: 700–716.
24. Jeoung J-H, Pippig DA, Martins BM, Wagener N and Dobbek H. *J. Mol. Biol.* 2007; **368**: 1122–1131.
25. Oohora K, Mashima T, Ohkubo K, Fukuzumi S and Hayashi T. *Chem. Commun.* 2015; **51**: 11138–11140.
26. Evans SV and Brayer GD. *J. Mol. Biol.* 1990; **213**: 885–897.
27. Komatsu T, Ohmichi N, Nakagawa A, Zunszain PA, Curry S and Tsuchida E. *J. Am. Chem. Soc.* 2005; **127**: 15933–15942.
28. Reddy KS, Yonetani T, Tsuneshige A, Chance B, Kushkuley B, Stavrov SS and Vanderkooi JM. *Biochemistry* 1996; **35**: 5562–5570.
29. Matsui T, Ozaki S, Liong E, Phillips GN Jr and Watanabe Y. *J. Biol. Chem.* 1999; **274**: 2838–2844.